Nuclear Instruments and Methods in Physics Research A271 (1988) 41–54
North-Holland, Amsterdam

STUDIES OF PHYSICS CONDITIONS FOR ANEUTRONIC AND/OR NONRADIOACTIVE NUCLEAR ENERGY GENERATION IN ^{3}He-INDUCED FISSION OF ^{6}Li AND ^{3}He FUSION IN A STEADY STATE MIGMA PLASMA *

Charles POWELL, James NERING, Bogdan C. MAGLICH and Austin WILMERDING

Aneutronic Energy Laboratory, United Sciences Inc., P.O. Box 3037, Princeton, New Jersey 08543, USA

The physical properties of a steady state migma plasma consisting of reacting ^{3}He, ^{6}Li, and d nuclei with densities $n \sim 10^{14}$ cm^{-3} and energies of 0.1–10 MeV, which corresponds to $\beta \geq 0.9$, were studied using a zero-dimensional collisional model and simulated by an iterative code on a CRAY computer (β does not have the same physical meaning here as in thermal plasmas). We conclude that if migma plasma can achieve the density currently attained in thermal plasma devices ($n \sim 10^{14}$ cm^{-3}), it will produce net energy through radionuclide-free aneutronic nuclear reactions with a power density of ~ 20 MW$_{th}$/m^3. Specifically: synchrotron radiation losses from multi-MeV migma are $\sim 10^3$ times lower than those from thermal plasma of the same density $n \sim 10^{14}$ cm^{-3}. We obtained a positive energy balance for the neutronless and radionuclide-free quasi-chain fission of ^{6}Li,

$$^3\mathrm{He} + {}^6\mathrm{Li} \rightarrow \mathrm{p} + 2\alpha + 16.9\ \mathrm{MeV}, \qquad \mathrm{p} + {}^6\mathrm{Li} \rightarrow \alpha + {}^3\mathrm{He} + 4\ \mathrm{MeV}, \tag{a}$$

and the pure ^{3}He fusion,

$$^3\mathrm{He} + {}^3\mathrm{He} \rightarrow \alpha + 2\mathrm{p} + 13\ \mathrm{MeV}, \tag{b}$$

with a "scientific" power output-to-input ratio $Q = 1.7$, as compared to the $Q \sim 10^{-3}$ obtained in thermal plasma. The radionuclide fraction or "radioactivity" $R = I_{rad}/I_t$ and a neutron power fraction or "neutronicism" $N = P_n/P_{nuc}$ are $R = 0.5\%$, $N = 2\%$ for (a), and $R = \mathrm{N} = 0.0\%$ for (b). For

$$\mathrm{d} + {}^3\mathrm{He} \rightarrow \alpha + \mathrm{p} + 18\ \mathrm{MeV} \tag{c}$$

in migma, we obtain $Q \sim \infty$, $R = 0.5\%$, and $N = 3.5\%$. Our results suggest that in the next stage of simulation, the 3-component fuel d + ^{3}He + ^{6}Li should be used to obtain high Q and, simultaneously, low R and N. For nonradioactive aneutronic migma: (a) bitemperature migma is essential; ignition is *not* possible in a Maxwellian system; (b) nor is ignition possible in a closed system (end losses are essential); (c) the diamagnetic well is essential; (d) the system must confine ions up to $E_i = 10$ MeV (15 MeV for D – ^{3}He protons); and (e) migma does not become thermalized, which makes a steady state reactor operation feasible.

1. Introduction

1.1. Statement of problem and definitions

Exoergic nuclear reactions *without* radionuclides or neutrons in the initial and final states have been known since the discovery of the proton-induced fission [1] of ^{7}Li: $\mathrm{p} + {}^7\mathrm{Li} \rightarrow 2\alpha + 17$ MeV. A number of similar "light fission" reactions in which a light nucleus (^{6}Li, ^{7}Li, ^{7}Be, ^{11}B, etc.) is split by protons or ^{3}He were subsequently discovered. Although the specific energy released in these reactions is about double that of uranium fission (2 MeV versus 0.8 MeV per nucleon), their use as a power source was not given serious consideration in the past due to:

(i) the absence of a reaction chain;

(ii) the lack of means to heat plasma to the multi-MeV energies required by the reactivities $\langle \sigma v \rangle$ of such reactions, which reach their peak at an ion energy $E_i \sim 2$ MeV;

(iii) the absence of confinement systems for multi-MeV ions with $Z > 1$; and, most importantly,

(iv) the inability to suppress a large electromagnetic radiation power loss from the reacting plasma, a loss that stemmed from the fact that the ion–electron power transfer $P_{ie} \propto Z^2$ and the nuclei involved have $2 \leq Z \leq 4$. The electromagnetic power radiated per unit volume of plasma, P_{em}, equals $P_b + P_s$, where P_b is bremsstrahlung and P_s is synchrotron radiation power per unit volume. In a high-temperature Maxwellian plasma, even if $\beta \sim 0.5$, P_s alone will exceed by orders of magnitude the power output per unit volume, P_{tot}, where $P_{tot} = P_{nuc} + P_{in}$, with P_{nuc} and P_{in} representing nuclear power generated and input power per unit volume. Since $P_s \gg P_b$, even in the special cases in which the reacting plasma would ignite against bremsstrahlung losses, it could not ignite against synchrotron losses [2].

There are two relatively new concepts, however, that show promise of solving or bypassing obstacles (i)–(iv).

* Research sponsored by the Air Force Space Technology Center (AFSC) under Contract F49620-85-C-0098.

First, the proposed proton–^{3}He chain fission of ^{6}Li (section 1.2) address problem (i); we will refer to it as the "quasi-chain". Second, the synthetic plasma consisting of "self-colliding orbits" or "migma plasma" has been experimentally and theoretically investigated; the results (sections 1.3 and 1.4) suggest that problems (ii), (iii), and (iv) might be circumvented if ion densities of the order of $n \sim 10^{14}$ cm^{-3}, attained at present in thermal plasma machines, can be attained in migma plasma.

The data presented below will summarize the results of investigations of the ^{3}He + d and ^{3}He + ^{3}He fusion and ^{3}He- and proton-induced fission reactions in migma plasmas carried out over the past decade or so. The studies delineate the general physical conditions required for the "scientific" power density output-to-input ratio, $Q = P_{tot}/P_{in}$, to exceed unity. Physical effects and experimental parameters that bear upon the attainment of $Q > 1$ are identified and examined, and avenues for the increase of Q are pointed out.

A reacting plasma will be defined as "nonradioactive" if the rate of production of radionuclides per unit volume in all primary and secondary reactions I_{rad} is less than 1% of the total nuclide output I_{tot}, that is, if the "radioactivity" $R = I_{rad}/I_{tot} < 0.01$. A reacting plasma will be termed "aneutronic" if the neutron power output per unit volume, P_n, is less than 1% of the total power output $P_{tot} = P_i + P_e + P_{em} + P_n$, where P_i, P_e, and P_{em} are the output power carried in unit volume by the ions, electrons, and electromagnetic radiation, respectively; i.e., if the plasma's "neutronicism" $N = P_n/P_{tot} < 0.01$. Migma is defined as "ignited" if $M = P_{tot}/P_{em} > 1 - \epsilon$, where $\epsilon < 1$ is the energy conversion efficiency. A plasma with $M > 1$ undergoes "self-ignition", i.e., it will experience a self-sustained burn on the basis of low-energy fuel injection alone without the necessity of recycling any part of the output power. A plasma with $1 > M > 1 - \epsilon$ undergoes "driven ignition", wherein part of the output power must be returned as fuel injection energy.

Throughout the paper, unless otherwise stated, all densities n are in units of 10^{14} cm^{-3}, rates I in 10^{14} cm^{-3} s^{-1}, energies E and temperatures T in MeV, power densities P in MeV cm^{-3} s^{-1}, and B in T.

1.2. Quasi-chain fission of ^{6}Li

The proton-induced two-step chain fission of ^{6}Li was proposed by McNally [3]:

$$p + {}^6\mathrm{Li} \rightarrow {}^3\mathrm{He} + \alpha + 4\ \mathrm{MeV}, \quad (1)$$

$$\uparrow\ {}^6\mathrm{Li} + {}^3\mathrm{He} \rightarrow 2\alpha + p + 16.9\ \mathrm{MeV}. \quad (2)$$

Its energy balance in a thermonuclear system was studied [4]. To differentiate it from the one-step chain in uranium fission, we will refer to the chain of the type (1), (2) as the "quasi-chain", because it can work only if the rate of reaction (2) is greater than that of reaction (1); such is generally not the case, but as we will show later, the difference could be made up for by other proton-producing reactions, as well as by the "chain subsidy".

The sequence (1), (2) can be written as the quasi-reaction

$$p + 2{}^6\mathrm{Li} \rightarrow 3\alpha + p + 20.9\ \mathrm{MeV}, \quad (3)$$

where the proton continues the chain. Quasi-reaction (3) can be made self-sustaining by the injection of cold ^{6}Li into an MeV plasma consisting of protons, ^{3}He, and α-particles. Unlike the case of uranium–neutron fission, there are *two* chain carriers [5] in reactions (1) and (2): p *and* ^{3}He. The theoretical multiplication factor κ for both p and ^{3}He is unity; in practice, owing to unavoidable losses, $\kappa < 1$ and the chain carrier density must be subsidized [6] by the injection of a small amount of both cold hydrogen and ^{3}He. The chain carriers, p and ^{3}He, play equivalent roles. Assuming similar cross sections for the two reactions, the reaction sequences (1) → (2) and (2) → (1) are interchangeable:

$$^3\mathrm{He} + {}^6\mathrm{Li} \rightarrow p + 2\alpha + 16.9\ \mathrm{MeV} \quad (2)$$

$$\uparrow\ {}^6\mathrm{Li} + p \rightarrow \alpha + {}^3\mathrm{He} + 4\ \mathrm{MeV}, \quad (1)$$

which can be written as the quasi-reaction

$$^3\mathrm{He} + 2{}^6\mathrm{Li} \rightarrow 3\alpha + {}^3\mathrm{He} + 20.9\ \mathrm{MeV}. \quad (4)$$

In the equilibrium reactor state, when the density of the

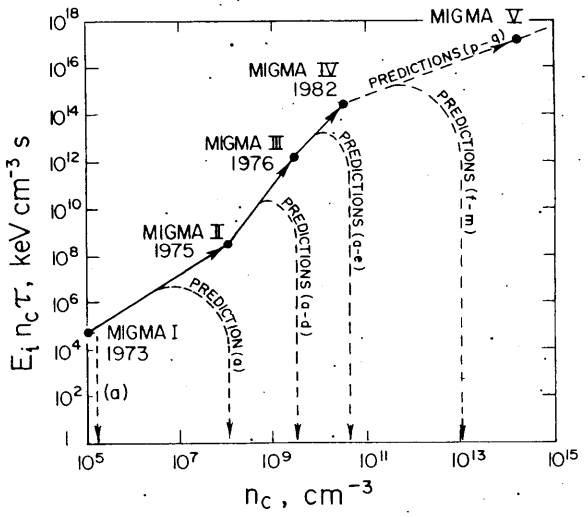

Fig. 1. Migma progress in terms of the product of ion energy, density, and containment time as a function of peak density. The downward arrows indicate degradation that would occur owing to instability. Letters (a)–(m) refer to instabilities listed in table. 1.

Table 1
Stability experience and expectations in migma experiments

Potential instabilities	Migma I	Migma II	Migma III	Migma IV	Migma V
Negative mass	×	×	×	×	×
Low frequency flute, $\omega_{pi}^2 \ll \omega_{ci}^2$			×	×	
Harris instability, $T > T_{11}$			×	×	
Loss cone, branch coupling electron waves with $n\omega_{ci}$			×	×	
Ion cyclotron resonant mode, medium density				×	
Low frequency flute, $\omega_{pi}^2 > \omega_{ci}^2$					×
Ion cyclotron resonant modes, high density					×
Ion counterstreaming (radial); ion–electron two stream					×
Loss cone convective, high-frequency branch					×
Drift cyclotron loss-cone					×
Ion beam/plasma (injection and exponentiation)					×
Precessional mode					×
Ballooning mode					×
Observations	none observed	none observed	none observed	moderate non-disruptive rf signal observed	
Stabilizing features	$P_\theta \sim 0$	$P_\theta \sim 0$	$P_\theta \sim 0$, short length, metal walls		$E_i > 0$, high T_e, metal walls, $P_\theta \sim 0$, short axial length, non-adiabatic z motion, precession and energy spread. (ref. [30])
	Migma equilibrium corresponds to minimum total effective potential energy (ref. [17])				
External stabilization techniques (refs. [31,32])	not used	not used	not used	E-field used	Line tying Image current Feedback

reactor products equals that of the fuel, quasi-chains (3) and (4) are indistinguishable.

From the point of view of nuclear physics, quasi-reactions (3) and (4) could be considered equivalent to the reaction

$$^6\mathrm{Li} + {}^6\mathrm{Li} \rightarrow 3\alpha + 21\ \mathrm{MeV}, \qquad (4)$$

"catalyzed" by protons. The protons act to lower the Coulomb barrier and effectively increase the rate of reaction (4). In the alpha particle model of nuclei, ^{6}Li is made up of an α and a deuteron. Hence, reaction (4) can be thought of as the virtual "photonless" process $d + d \rightarrow \alpha + 24$ MeV in the presence of two "spectator" alpha particles that conserve the momentum. Therefore the photon is not required and the cross section for the $dd \rightarrow \alpha$ reaction becomes $(e^2/hc)^2 = 137^2 \sim 10^4$ times greater than in the stellar cycle.

1.3. Self-colliding orbits ("migma plasma")

In the mid-1970s, the concept of self-colliding orbits, which originated in high energy physics studies [7], was used to demonstrate experimentally that a "synthetic" MeV plasma can be made without heating. Accelerated ions were injected into a simple mirror to form the

Table 2
Comparison of physical parameters of a mirror containing plasmas to those containing self-colliding orbits (migma)

Physical configuration and Parameters	Plasma mirror	Self-colliding beam mirror (Migma)
Orbit characteristics	adiabatic orbits; gentle variations of B along the particle trajectories	non-adiabatic orbits; large variations of B along the orbits
Radial scale length of the magnetic field $R_M = \left\lvert \frac{dr}{dB} B \right\rvert$	$R \ll R_M$	R_M comparable to R_{ci}
Ion Larmor radius R_{ci} compared to plasma radius R_p	small, $R_{ci} \ll R_p$	large, $R_{ci} \sim \frac{1}{2} R_p$
Canonical ang. mom. $P_\theta = m_i r \left\langle v_\theta + \frac{eA_\theta}{m_i c} \right\rangle$	large; broad distribution	≈ 0 (orbits through or near the axis of symmetry)
Radial scale length of density $a = \left\lvert \frac{dr}{dn} n \right\rvert$	$a \gg R_{ci}$	$a < R_{ci}$
Axial extent	long, many fold R_{ci}	short, comparable to R_{ci}
Distribution of motions	random (quasi-Maxwellian, of loss-cone type)	quasi-ordered, with large dispersion due to precession, z-oscillations and multiple scattering

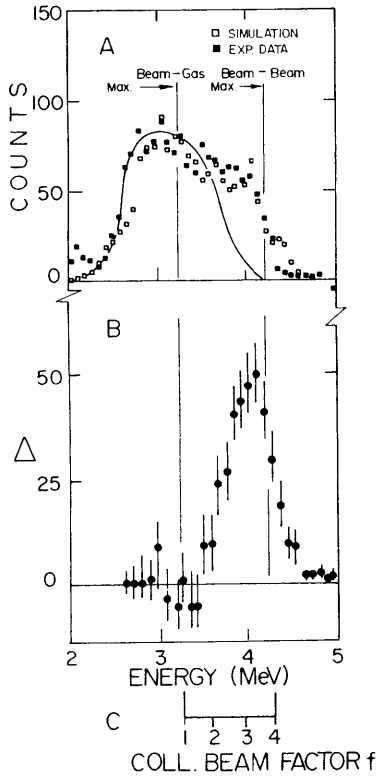

"self-colliding" orbit pattern in the presence of ambient cold electrons [8,9]. This "self-collider" has provided stable confinement of 0.8 MeV ions [6] at low density [10,11]. Both the ion energy and density have thus far been limited by the injection current and the magnetic field of the particular devices used; none of the instabilities observed or predicted for thermal plasmas has been observed in migma plasma. Progress in terms of the triple product $E_i n \tau$ (ion energy × density × confinement time) as a function of the central migma density n_c is shown in fig. 1. Table 1 lists the instabilities that might have been expected but were not seen in migmas. I–IV.

The ion motions in migma plasma are quasi-ordered and highly non-Maxwellian ("nonthermal"). The center-of-mass energy between a pair of like ions is as much as 3–4 times that in the Maxwellian distribution, i.e., the $\langle E_{CM} \rangle_{migma} = k \langle T_i \rangle$, with $1.7 < k < 2$ as opposed to the Maxwellian $\langle E_{CM} \rangle = \frac{1}{2} \langle T_i \rangle$ (fig. 2). Due

Fig. 2. Colliding beam factor. (A) Observed proton energy distribution from d+d is a superposition of beam-on-gas (approximate curve A) and beam-on-beam (solid and hollow squares). (B) The difference Δ between experimental points (solid squares) and curve A. (C) The colliding beam factor f ranges from 1 at the beam-on-gas maximum to 4 at the beam-on-beam maximum.

to the "decoupling" effect [12], the electron temperature in migma, T_e, is always lower than the ion kinetic energy E_i; typically, $T_e/E_i \leq 0.1$. The electron motion is not known but is believed to be Maxwellian in the central zone and quasi-ordered at the periphery. Other differences between migma and thermal plasmas are shown in table 2. Due to a property of central orbits [13] (zero canonical angular momentum), the negative mass instability, which limited the plasma density in simple mirrors to 5×10^5 cm^{-3}, was not evident in a migma at $n_c \sim 10^{10}$ cm^{-3}.

1.4. Migma diamagnetic well

As the diamagnetic parameter β approaches unity, the migma ions will depress the zero order magnetic field, creating a diamagnetic well [14]. Migma diamagnetism converts the maximum B field of a simple mirror into a minimum B field (fig. 3). The shape of the magnetic well was calculated self-consistently for a 2-dimensional system by several independent methods [15–19]. It implies an on-axis β_0 (defined in terms of the net field) $\gg 1$ and, consequently, a large mirror ratio, crucial for the confinement. A 90% diamagnetic depression, $B/B_0 = 0.1$, which implies a mirror ratio of 10, was experimentally observed with large orbits [20] in 2XIIB. Our model however, treats confinement not in terms of mirror ratio but in terms of the mirror "confinement factor", which is assumed to be 0.1 (section 2).

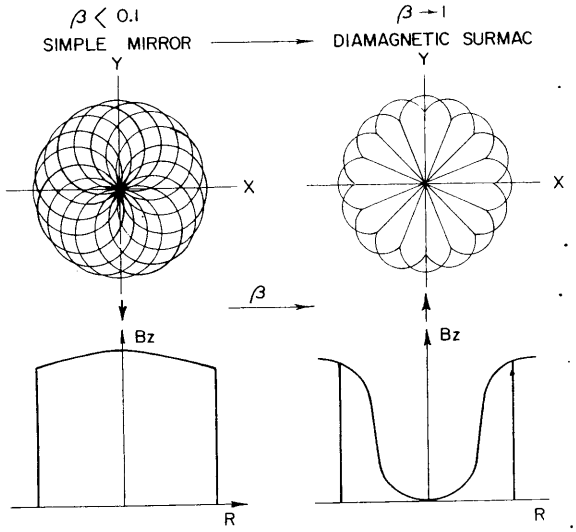

Fig. 3. Effect of the diamagnetic field of migma on the net magnetic field: the external simple mirror (B_{max}) field (left) is practically unchanged for $\beta < 0.1$, but at higher migma densities a diamagnetic well is created whose depth increases as β approaches unity. At $\beta \approx 1$, the magnetic field is nonzero only at the periphery of the migma (diamagnetic surmac). The orbit trajectories in the field-free region become linear.

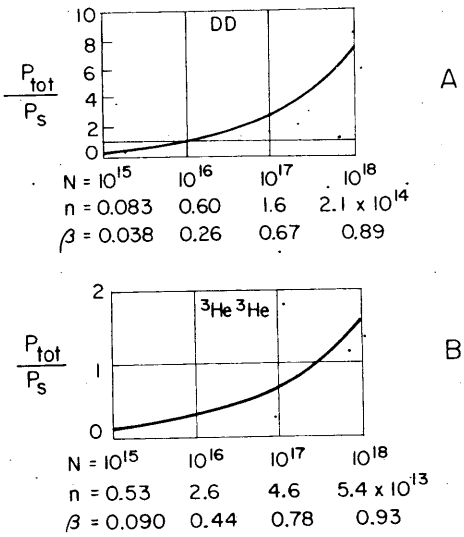

Fig. 4. Monte Carlo simulation of P_{nuc}/P_s as a function of particle linear density N (cm^{-1}), volume density n (cm^{-3}), and β for a migma reactor fueled with (A) deuterons at 1 MeV and (B) ^{3}He at 4 MeV. A vacuum field of 7 T was used for this calculation.

In addition to the large mirror ratio, the migma diamagnetic well serves to suppress substantially synchrotron radiation loss P_s, thus making $P_{em} < P_{tot}$. Synchrotron radiation power density can be written [21] as

$$P_s = 0.39 B^2 T_e n_e \phi, \tag{5}$$

where n_e and T_e are electron density and temperature, B is the magnetic field inside the plasma, related to the vacuum field B_0 by $B = B_0(1-\beta)^{1/2}$; and $\beta = 1 - (B/B_0)^2$. ϕ is the absorption correction, which is a function of the geometry, always less than 1. The decoupling effect [12] in migma reduces P_s by an order of magnitude [22] from its level in a thermalized plasma. Monte Carlo simulations [22] of a 1 MeV pure d migma and a 4 MeV pure ^{3}He migma show that $P_{tot} \geq P_s$ for $\beta \geq 0.26$ and $\beta \geq 0.85$, respectively (fig. 4). An analytic calculation based on a simple model of migma [23] that includes upper harmonics suggests ignition against synchrotron radiation for reaction (1) when $B/B_0 < 0.1$, i.e. $\beta = 0.990$, with $\phi = 1$. In our simulation we used the product $(B/B_0)\phi = 0.9999$, which is equivalent to either $\beta = 0.90$, $\phi = 0.0316$, or $\beta = 0.9999$, $\phi = 1$.

For the extreme (second) case, Burkhardt has offered a heuristic physical picture of synchrotron radiation and derived a formula for P_s [24].

Since P_s rapidly approaches zero as $\beta \to 1$ and $P_s = (1-\beta)^{3/2}$, the synchrotron radiation subsides and is replaced by the much weaker surface radiation whose power density is *Independent* of the vacuum magnetic field B_0 and is given by [24]

$$P_s' = S(6 \times 10^{-8}) n_e^{3/2} T_e^2. \tag{6}$$

$P_s' \ll P_b$ as long as $T_e^3/n_e < 2\times10^{-5}\ R^2$, where R is the migma radius in cm and S is the parameter that measures deviation from the ideal surface radiation, which corresponds to $S=1$. Our parameter $(B/B_0)\phi = 0.9999$ is equivalent to $S=625$, which gives a surface radiation from an $R=60$ cm migma with $n_e=5$ equivalent to a P_s with $\langle B\rangle \sim 13R^{-7/4} \sim 0.01$. For a vacuum field $B_0=10$, this implies a synchrotron radiation power loss lower by six orders of magnitude than that given by eq. (5). The degree to which P_s can be replaced by P_s' will depend upon the magnetic field penetration into the migma surface.

2. Classical model of reacting migma

To determine if the chain fission process of ^{6}Li (eq. (3) or (4)) could be ignited with net nonradioactive and/or aneutronic power production, the classical processes in a primary migma plasma consisting of p, ^{3}He, and ^{6}Li, as well as the migma plasma of the nuclear reaction products (referred to as the "secondary migma") were studied. The beta values of the migma plasma were assumed to be in the range 0.85–0.95; due to the high ion energy (1–10 MeV), such are reached already at the densities $n \sim 10^{14}$ cm^{-3}.

A zero-dimensional model of a migma was simulated using a multigroup iterative code run on a CRAY-1 computer. The model assumes a 100% confinement for ions with $E_i \le 0.1$ (by means of plugs or ambipolar potential) and particle losses for $E_i > 0.1$. Particle losses are due solely to ion Coulomb scattering into the loss cone; each exiting ion is accompanied by an electron of temperature T_e. We computed the deceleration rate and the perpendicular and parallel diffusion rates between test (j) and field (k) particles [25], with Λ set equal to 11. The loss rate per cm^3 is $CI_\perp$, where $I_\perp$ is the 90° scattering rate of the jth by the kth ion, and C is the confinement factor. For perfect confinement, $C=0$; more typically, $C=0.1$. Twenty-five nuclear reactions [26] were included (table 3). A major impediment to this study was the lack of cross section data above 1 MeV for all of these reactions, coupled with the fact that (as will later be shown) the ions have to be confined up to 10 MeV. The reactances $\langle\sigma v\rangle$ were fitted to an exponential function, in terms of the ion energy E_i, of the form AE_i^D, where A and D are constants for $E_i \le 2$ and set constant ($D=1$) for $E_i \ge 2$ (fig. 5). The value of P_b was computed relativistically [19]. For synchrotron losses, since our β was between 0.9 and 1, we used eq. (6) multiplied by a factor $S=625$. This was equivalent to using eq. (5) with $B=0.1$, which is 10^2 times lower than B_0, but 10 times higher than the equivalent B producing the same P_s'. Since our model is a "point" in space (zero-dimensional), ϕ was set to 1. A real, physical ϕ is less than unity, thus our model *overestimates* P_s

Table 3
Nuclear reactions used in the BEBE situation

1	^{3}He + ^{3}He	→	2p + α + 12.861
2a	d + d	→	p + T + 4.032
2b		→	^{3}He + n + 3.267
3	d + T	→	α + n + 17.586
4	T + T	→	α + 2n + 11.327
5	T + P	→	n + ^{3}He − 0.764
6	d + ^{3}He	→	p + α + 18.351
7a	T + ^{3}He	→	d + α + 14.319
7b		→	p + α + n + 12.092
8a	d + ^{6}Li	→	^{7}Be + n + 3.380
8b		→	^{7}Li + p + 5.026
8c		→	p + α + T + 2.561
8d		→	2α + 22.374
8e		→	^{3}He + α + n + 1.796
9a	^{3}He + ^{6}Li	→	p + 2α + 16.880
9b		→	d + ^{7}Be + 0.113
10	p + ^{6}Li	→	^{3}He + α + 4.022
11	d + ^{7}Be	→	p + 2α + 16.769
12	T + ^{7}Be	→	p + 2α + n + 10.510
13	^{3}He + ^{7}Be	→	2p + 2α + 11.274
14a	^{6}Li + ^{6}Li	→	^{11}B + p + 12.218
14b		→	^{7}Be + α + n + 1.908
14c		→	3α + 20.901
14d		→	^{11}C + n + 9.453
14e		→	^{10}B + d + 2.987

appropriate to a deep diamagnetic well. Radiation transport, absorption, and reflection, usually contained in ϕ, are not included in eq. (5) or (6); furthermore, eq. (5) assumes that electron motions are always perpendicular to the magnetic field.

The code performs 10^4–10^5 physical parameter computations per 10^{-3} s time step. Changes in n_i as the E_i-distribution changes (owing to energy transfers,

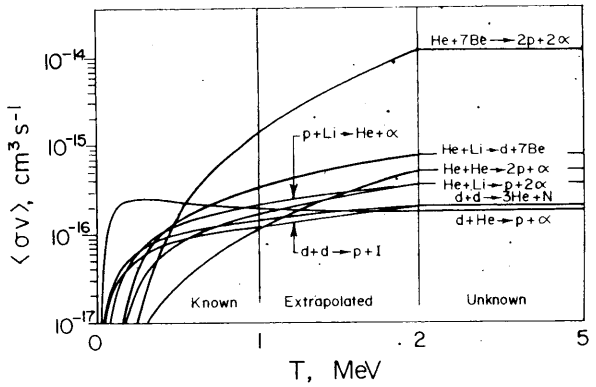

Fig. 5. Maxwellian reactivity $\langle\sigma v\rangle$ as a function of T, defined as $\frac{2}{3}$ of the average total reacting particle energies. The reactivities for $0 < T < 1$ are taken from published results. For $1 < T < 2$, the reactivities are extrapolated by curve fit. For $2 < T < 5$, the reactivities are taken as constant and equal to their values at $T=2$.

reactions, ion injection and escape, P_s, P_b, hot electron escape, and cold electron injection with ions) are facilitated by selecting, from among 125 energy bins, the n_i for each given E_i and, for nuclear reactions, by changing the ion species.

We summarize the main features of the model thus:

(1) A 100-keV end plug potential is assumed.
(2) T_e is an initial adjustable parameter on the order of 10 keV.
(3) Charge neutrality is assumed: $Zn_i = n_e$.
(4) Mirror losses are accounted for by the use of a confinement enhancement factor: T(confinement) $= T(90°)$ divided by a confinement factor C, where $C = 0$ denotes perfect confinement and $C > 0$ denotes loss-cone leaks.
(5) Ions are confined with energy up to 10 MeV.
(6) Ion–ion and ion–electron energy transfer (dynamical friction) are included and adjustable.
(7) Synchrotron radiation power is assumed to be given 625 times the surface radiation P_s' given by eq. (6).
(8) Bremsstrahlung is described by a relativistic electron model.
(9) Cross sections are taken as $\sigma = AE_i^D$ for $E_i > 1$.

3. Test of the model

3.1. Time structure of ion injection

Our model was tested using

$$d + {}^3He \rightarrow \alpha + p + 18.4\ MeV, \qquad (7)$$

which is believed to ignite below 100 keV [3,27–31]. At $t = 0$, the "reactor" is already filled with d and ^{3}He of equal densities $n_{20} = n_{30} = 3$, and energies $E_{20} = 0.025$ and $E_{30} = 0.2$; i.e., the fuel mix, defined as the ratio $\gamma = {}^3He:({}^3He + d)$, is 1 : 2. The electron distributions are Maxwellian with an initial temperature $T_e = 0.01$ and density n_e as required for neutralization. Beginning at $t = 0$, a dc injection of d and ^{3}He of the same energy is added to the initial particle population n_{i0} at a rate of $0.15n_{i0}$ s^{-1}. It can be shown [32,33] using the second law together with the standard ion–ion and ion–electron power transfer relations [25] that the ion energy distribution will evolve from the monoenergetic state at $t = 0$ into *two* energy peaks at the time of ignition: (a) the reacting fuel ions, whose energy distribution should be centered at the reaction ion energy $E_{ir} = 0.025$, and (b) the hot secondary migma (the reaction products) at $E_{ih} \geq 1$. As required by thermodynamic considerations, the latter serves as the "hot reservoir" that supplies energy to the fuel ions to perform the work of overcoming the low temperature ion and electron drag. Observation of a two-temperature distribution would be a *critical test* of the reliability of our simulation technique. Obtaining ignition without two-temperature distribution would imply a perpetuum mobile of the second kind.

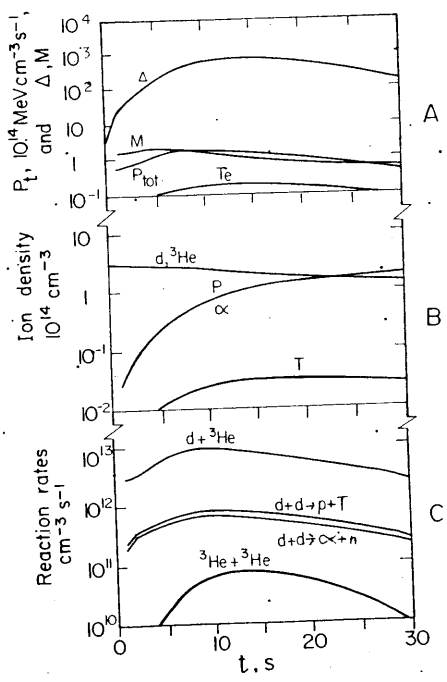

Fig. 6. Closed system fails to ignite. Reactor parameters for d + ^{3}He and associated reactions as a function of time, for $C = 0$ (closed loss cone), P_{nuc} is the total power; $M = P_{nuc}/P_b$; Δ in the normalized system energy content.

If we label the average energy content of the fuel ions $\langle E_{ir} \rangle$ and that of the electrons $\langle T_e \rangle$, the energy contained in the cold reservoir is $q_2 = \langle E_{ir} \rangle + \langle T_e \rangle$ and that of the hot reservoir, due only to ions, is $q_1 = \langle E_i \rangle$, since $T_e \ll 1$ MeV. The thermodynamic work equals $q_1 - q_2$, and the thermodynamic efficiency is given by

$$\eta_{th} = 1 - q_2/q_1. \qquad (8)$$

For a single reservoir, $q_2 = q_1$ and $\eta_{th} = 0$ (second part of second law). In terms of eq. (8), the critical test requires that $q_1 > q_2$.

3.2. Failure to ignite a perfectly confined migma

The d + ^{3}He migma system with the loss cone closed, $C = 0$ (perfect confinement), failed to ignite. The energy content gradually increased initially, but the buildup of unremoved ash (α-particles) damped the reaction rate while increasing the P_{em} rate; the energy content began to decrease after 10 s and fell to the initial value at 40 s (fig. 6).

3.3. Open loss cone and evolution of reacting migma

The situation was radically changed by opening the loss cone, $C = 0.1$. Four stages of the evolution of the

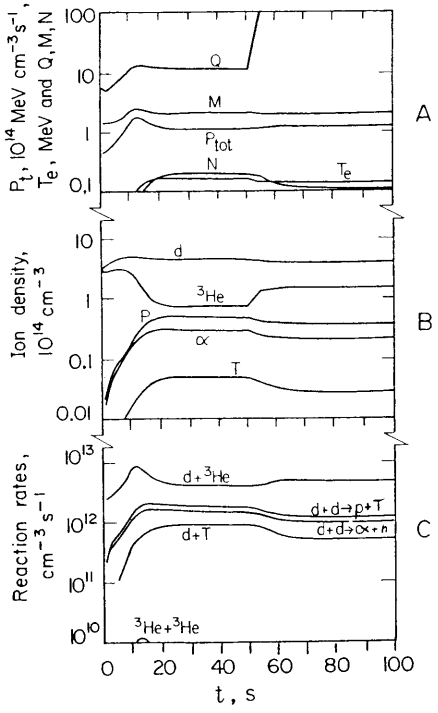

Fig. 7. Evolution of d + ^{3}He and migma; power generation parameters versus time. P_{nuc} is the total power; $N = P_n/P_{nuc}$, $M = P_{nuc}/P_b$. Open loss cone $C = 0.1$. Steady state self-ignition with $Q = 1.1 \times 10^5$ is reached after 70 s.

reacting migma have been observed (fig. 7): (i) in the transient state of "driven" injection, i.e., energized fuel (0–15 s), the distributions spread in velocity space and the reaction products with energies up to 20 MeV are kept in to heat d and ^{3}He and replenish the energy lost through radiation and particle end losses. (ii) In steady state driven ignition (15–50 s) all parameters become constant. (iii) in the transient state of cold fuel injection (50–70 s) the dc injection energy is lowered to approximately 10 eV, corresponding to gas or pellet injection. The lowest particle energy modelled by the code is 0.01 MeV, which is equal to the "bin" size (interval in the diagram); the computed $Q = 111$ is to be multiplied by 10^3. (iv) In the steady state self-ignition (70 s → ∞) phase a new equilibrium is reached.

Almost all the power generated in the d + ^{3}He system comes from the primary d + ^{3}He reactions and the d + d reactions (fig. 7c):

$$d + d \rightarrow T + p + 4\ \text{MeV}, \tag{9}$$

$$d + d \rightarrow {}^3\text{He} + n + 3.3\ \text{MeV}. \tag{10}$$

The d + T reaction rate is about half that of the combined (7) + (9) + (10) rate and is the main source of neutrons. The secondary reaction

$$^3\text{He} + {}^3\text{He} \rightarrow \alpha + 2p + 13\ \text{MeV} \tag{11}$$

has a negligible rate (0.33% of d + d).

3.4. Critical thermodynamical test

The ion energy spectrum at stage (iv) shows that a clear two-group structure has evolved from the original delta-function distribution: the reacting fuel ions with energies below 1 MeV and the "hot reservoir" ions with energies in the range 1–10 MeV (fig. 8A). The ratio of the energy content of the two reservoirs from fig. 9A is approximately

$$q_2/q_1 = 1/20, \tag{12}$$

and the thermodynamic efficiency, eq. (8), is

$$\eta_{th} = 0.945. \tag{13}$$

While the P_{em} losses will, of course, considerably reduce the overall efficiency, eq. (13) is nevertheless a measure of the level of ignition, as will be seen in the cases of driven ignition below.

3.5. Optimization of the fuel mix

Since N is proportional to the deuteron content, we reduced the neutron power P_n in a self-ignited d + ^{3}He reactor to a minimum by increasing the ^{3}He : d fuel ratio. The neutron energy spectra are shown in fig. 10. The effect of "deuteron leaning-out" of the fuel mixture

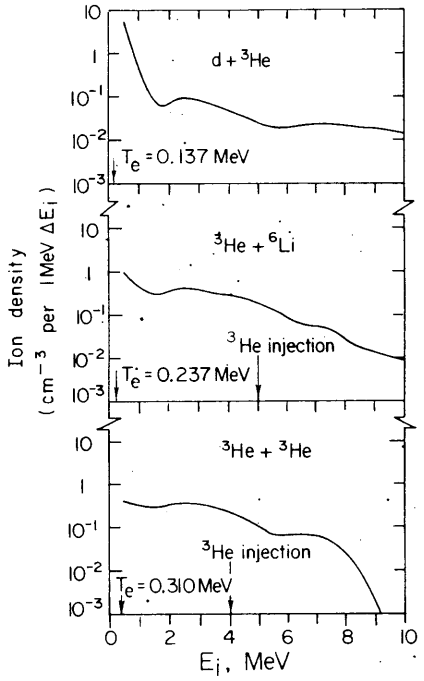

Fig. 8. Ion energy spectra. Ion density per 1-MeV energy interval as a function of ion energy for (A) d + ^{3}He, (B) ^{3}He + ^{6}Li, and (C) ^{3}He + ^{3}He systems. Electron temperature T_e for each system is given. ^{3}He injection energy for (A) is 10 keV.

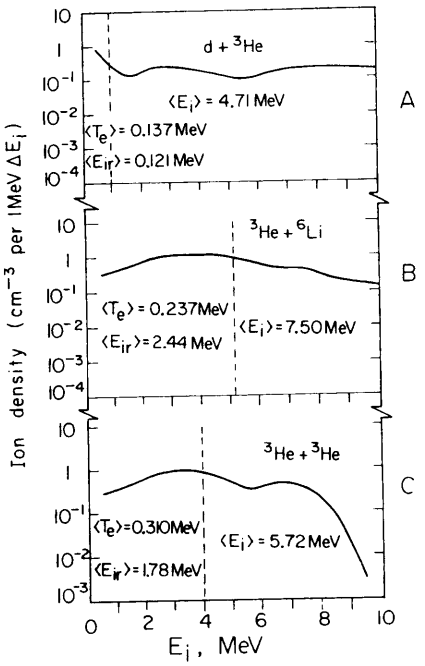

Fig. 9. Ion energy spectra. Ion density per 1-MeV energy interval as a function of ion energy for (A) d + ^{3}He, (B) ^{3}He + ^{6}Li, and (C) ^{3}He + ^{3}He systems. $\langle T_e \rangle + \langle E_{ir} \rangle$ and $\langle E_i \rangle$ comprise the average energy contents of the cold and hot reservoirs respectively and are used to define q_1 and q_2 in eq. (8). The dashed lines denote the boundaries between hot and cold reservoirs in each system.

can be seen in fig. 11. Here we plot the reduction of total power P_{tot}, the total neutron power P_n, and the neutron power associated with high-energy neutrons arising from the d + T reaction, P_n'. The quantities are plotted as a function of the fraction of ^{3}He in the injected fuel, $\gamma = {}^3\text{He}:({}^3\text{He} + \text{d})$. It is interesting to note that as γ is increased from 0.5 to 0.7, P_n and P_s' both fall off faster than P_{tot}. By trading off reactor power for a lower neutron power fraction $N = P_n/P_{tot}$, N can be reduced to $(3.5 \pm 3)\%$ at $\gamma = 0.7$. As the

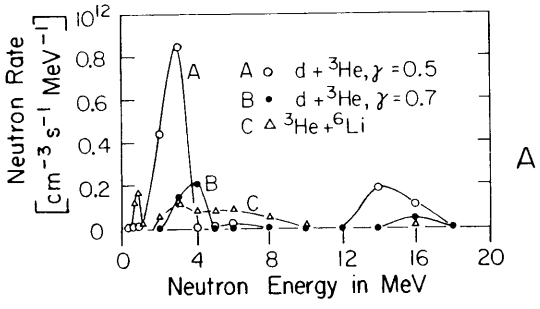

Fig. 10. Neutron energy spectra at $t = 50$ s for d + ^{3}He and ^{3}He + ^{6}Li migma.

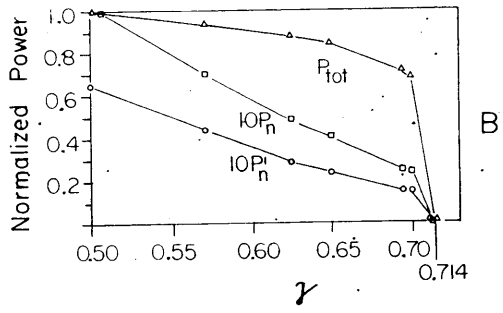

Fig. 11. Total reaction power P_n and neutron power P_n' from d + T as a function of the fractional proportion of ^{3}He in the fuel, $\gamma = {}^3\text{He}:({}^3\text{He} + \text{d})$. P_{nuc} and $10P_n$ are normalized to unity for $\gamma = 0.5$ (d = ^{3}He). For $\gamma > 0.71$, the reactor does not ignite but may be "driven".

system is leaned from $\gamma = 0.5$ to $\gamma = 0.7$, total power output drops by about 30%, whereas the neutron power output is reduced by about a factor of 5 (fig. 11).

The power flow diagram is shown in fig. 12. The input and output power parameters of the system are: $P_{in} = 8 \times 10^{-6}$ (0.00013 MW m^{-3}) and $P_{out} = P_{tot} = 1.13$ (18.08 MW m^{-3}). Hence, $Q = 1.1 \times 10^5$. P_{out} consists of the electron power $P_e = 0.16$; $P_s = 0.58$, $P_s = 0.004$, the power through the loss cone $P_{lc} = 0.26$, and the neutron power $P_n = 0.126$ (curve A in fig. 10).

Other parameters are: $M = P_{tot}/P_{em} = 1.89$; $P_s/P_b = 0.007$ and 0.25 for $B = 0.1$ and 0.5 respectively; $T_e = 0.132$ (fig. 7A); $C = 0.1$.

4. Chain fission of ^{6}Li

Our attempts to obtain the quasi-chain sequence (1) → (2), quasi-reaction (3), failed because of the low energy release from reaction (1). The evolution parameters displayed features similar to that for the perfect confinement case for d + ^{3}He (fig. 6). The reaction sequence was then reversed according to quasi-reaction (4), and net power was produced.

4.1. Parameters

The best initial conditions were found by trial and error: $\gamma = {}^3\text{He}/({}^3\text{He} + \text{Li}) = 0.37$; $n_{30} = 0.48$, $n_{60} = 0.71$, $E_{30} = 5$, and $E_{60} = 0.01$. The high minimal ^{3}He injection energy of 5 MeV required to produce ignition is associated with the high values of P_{em} and the small reaction cross section. The rate of the ^{3}He dc injection is $0.31 n_{30}$ s^{-1}, and that of ^{6}Li is $0.27 n_{60}$ s^{-1}. The "transient driven" stage lasts 35 s, after which the system settles down to a *steady state driven ignition* (see fig. 13A). The power flow parameters, with $C = 0.1$, are $P_{in} = 0.75$ (12.0 MW m^{-3}) and $P_{out} = 1.3$ (21.2 MW

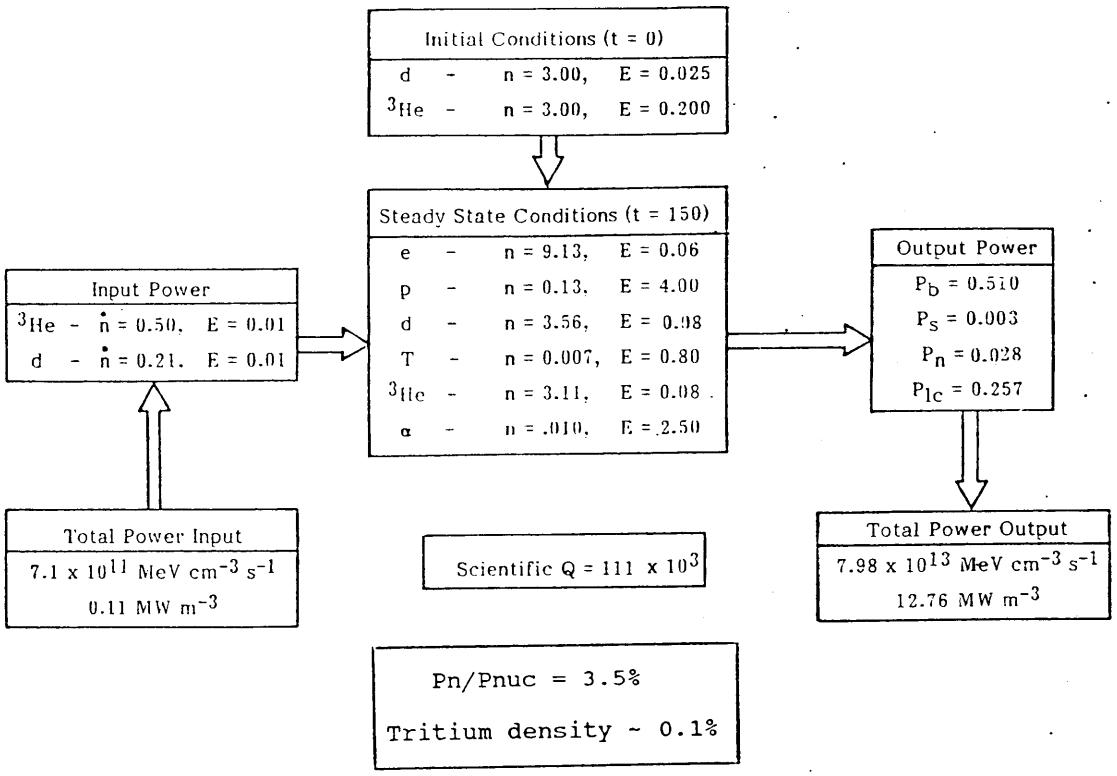

Fig. 12. Power flow diagram for d+^{3}He with the fractional proportion of ^{3}He in the fuel $\gamma = 0.7$. Densities n are in units of 10^{14} cm^{-3}, energies E are in MeV, input rates $\dot{n}$ in 10^{14} cm^{-3} s^{-1}, power outputs P in MeV cm^{-3} s^{-1}, and time t in s. Note that although the total power output in this case is only 30% less than that for the $\gamma = 0.5$ case (fig. 10), the neutron power output has dropped to about $\frac{1}{5}$ of that obtained in the $\gamma = 0.5$ case.

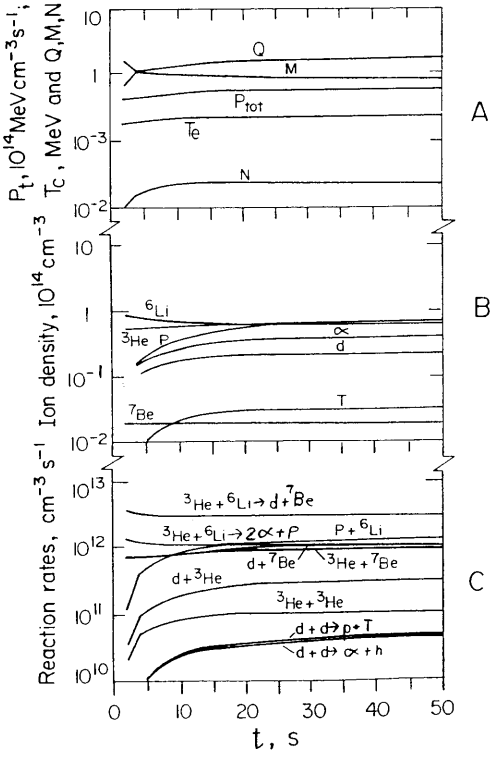

m^{-3}). Hence, $Q = 1.77$. P_{out} is composed of $P_e = 0.21$, $P_b = 0.70$, $P_s = 0.004$, $P_{lc} = 0.593$, and $P_n = 0.03$. The power flow diagram is shown in fig. 14. Self-ignition could *not* be achieved because of the high $E_{30} = 5$ MeV and the resulting high $T_e = 0.241$ and low $M = 0.86$.

The bi-temperature spectrum was again observed (critical test) (figs. 8B and 9B), but with $q_2/q_1 = \frac{1}{3}$ and, hence, a thermodynamic efficiency of

$$\eta_{th} = 0.67, \qquad (14)$$

which is $\frac{1}{3}$ lower than that for the self-ignited test reaction (7).

4.2. Secondary reactions

Unlike the d+^{3}He case, there is a concurrent primary reaction

$$^3\mathrm{He} + {}^6\mathrm{Li} \rightarrow \mathrm{d} + {}^7\mathrm{Be} + 0.11\ \mathrm{MeV} \qquad (15)$$

Fig. 13. Reactor parameters of the ^{3}He+^{6}Li system as a function of time. Steady state driven ignition is reached after 30 s. P_{nuc} is the total power, $M = P_{nuc}/P_b$, $N = P_n/P_{nuc}$. Open loss cone $C = 0.1$.

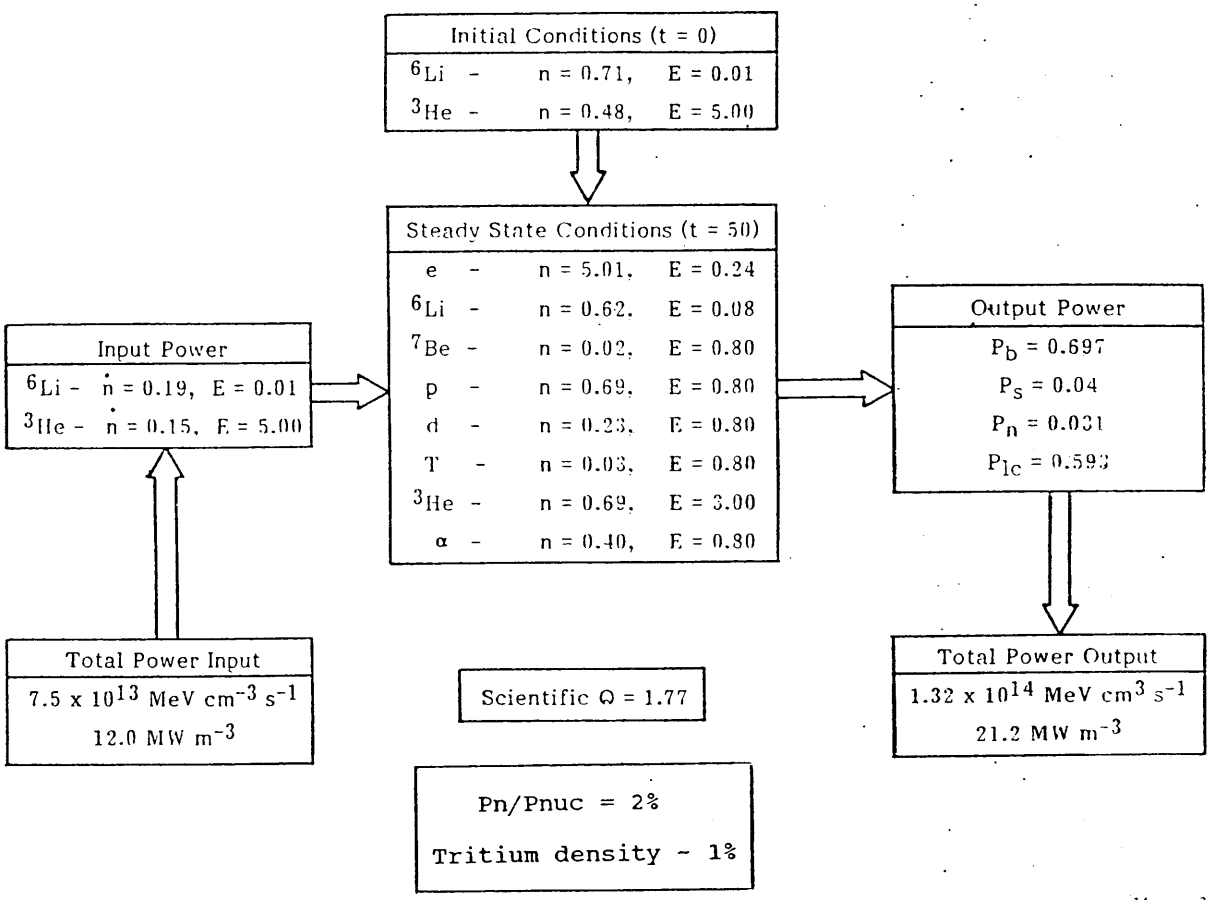

Fig. 14. Power flow diagram for $^3He+^6Li$. Densities n are in units of 10^{14} cm^{-3}, energies E in MeV, input rates $\dot{n}$ in 10^{14} cm^{-3} s^{-1}, power outputs P in MeV cm^{-3} s^{-1}, and t in s.

that has a higher rate than the primary one, reaction (2) (fig. 13C). Furthermore, concurrent with reaction (2) are the secondary reactions (1) and

$$^3He + {}^7Be \rightarrow 2p + 2\alpha + 11.3\ \text{MeV}, \quad (16)$$

$$^3He + d \rightarrow \alpha + p + 18\ \text{MeV}. \quad (17)$$

The rate of reaction (11) is now 10% of the primary reaction rate; however, the contribution of reactions (9) and (10) has dropped to 1%.

Although no protons are injected, the ^3He–^6Li migma evolves into a partial $p+^6Li$ migma, and the *chain* reactions (1) and (2) take place (see rates in fig. 13C). Assuming equal rates, we can qualitatively describe the chain consisting of reactions (2), (15), (16), (17), and four reaction (1)'s as the quasi-reaction in which four ^3He's "catalyze" the transformation of six ^6Li nuclei into 9α:

$$4\,^3He + 6\,^6Li \rightarrow 9\alpha + 4\,^3He + 62\ \text{MeV}, \quad (18)$$

(the $4\,^3He$ are recycled)

again generating 10 MeV per ^6Li. A glance at fig. 13C suggests that an increase of the rate of reaction (7) by a factor of 2–3 and/or that of reaction (10) by the same factor might result in self-ignition. This possibility exists since, owing to the lack of data on the cross sections of the two reactions between 1 and 5 MeV (the energy of most of the ^3He and deuterium – see fig. 9B), the rates of these two reactions were set artificially low (fig. 5). Because their average Zs are 1.5 and 2, respectively, reactions (7) and (10) have lower P_{em} than (2), (15), (16), and (17), in addition to high energy release.

Clearly, the Q of the ^3He chain critically depends on the magnitude of the cross sections for the $d+^3He$ and/or $^3He+^3He$ reactions.

5. ^3He–^3He fusion (reaction (11))

We have simulated a reactor based on reaction (11) alone to investigate its properties. The best initial conditions were found to be: $n_3 = 0.60$, $E_{30} = 4$; the ^3He dc injection occurs at a rate of $0.075 n_{30}$ s^{-1}. As illustrated

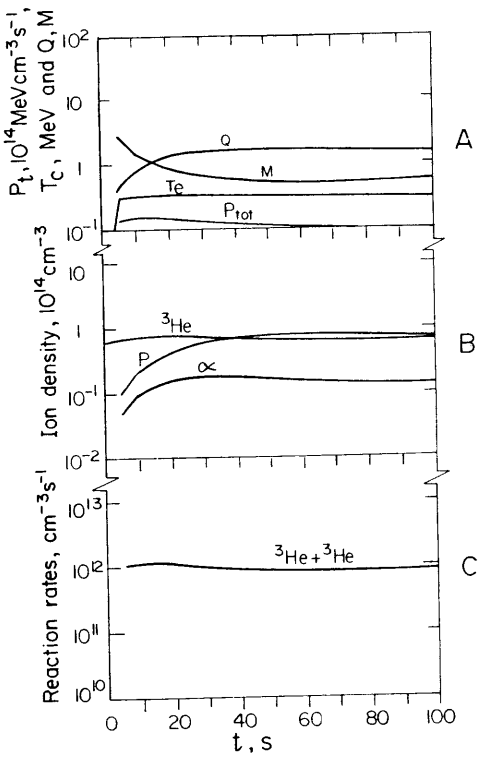

Fig. 15. Reactor parameters of the ^{3}He+^{3}He system as a function of time. Steady state driven ignition is reached after 40 s. P_{nuc} is the total power, $M = P_{nuc}/P_b$. Open loss cone $C = 0.1$.

in fig. 15A, the transient driven stage lasts 50 s, after which the system settles down to a steady state driven ignition, with $P_{in} = 0.18$ (2.88 MW m^{-3}); $P_{out} = 0.29$ (4.1 MW m^{-3}). Hence, $Q = 1.58$. P_{out} is composed of $P_e = 0.028$, $P_b = 0.19$, $P_s = 0.003$, $P_{lc} = 0.066$, and $P_n = 0.0$. The power flow diagram is shown in fig. 16. As in the case of ^{3}He + ^{6}Li, self-ignition could not be achieved because of the higher $E_{30} = 4$, the high $T_e = 0.310$, and low $M = 0.56$.

The reaction is both *absolutely nonradioactive* ($I_{rad}/I_t = 0$) and *absolutely aneutronic*: $P_n/P_{nuc} = 0\%$ when only the dominant reactions are taken into account (reactions (1), (6), (8), (9), (11), and B from table 3). The two-temperature groups were observed (critical test) (see figs. 9A and 9B, but with $q_2/q_1 = 1.98/5.72 = 0.3$, $\eta_{th} = 0.67$. (19)

We note: (1) The optimal E_{30} is lower by 1 MeV than that for the ^{3}He + Li reactor; this is a result of the lower average Z, so that P_{em} is lower. (2) The reaction rate is lower than that for ^{6}Li reactions; however, a cross section increase by a factor of 3 at 4 MeV would make them equal.

6. Conclusions

6.1. Ignition physics

The simulation "experiments" have provided us with the following insights into ignition physics conditions:

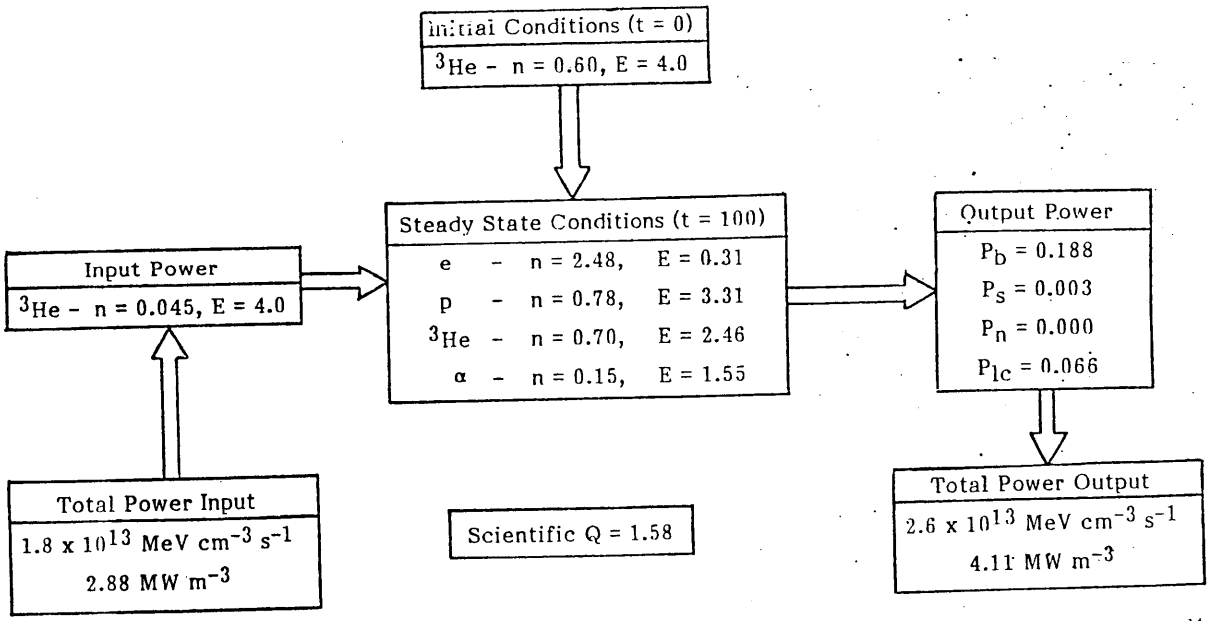

Fig. 16. Power flow diagram for ^{3}He+^{3}He. Densities n are given in units of 10^{14} cm^{-3}, energies E in MeV, input rates $\dot{n}$ in 10^{14} cm^{-3} s^{-1}, power outputs P in MeV cm^{-3} s^{-1}, and t in s.

(a) Ignition is incompatible with a thermalized, Maxwellian migma. Bi-temperature migma with thermodynamic efficiency of the order of 1 is essential for self-ignition and with efficiency of $\frac{2}{3}$ for driven ignition. (b) The primary migma (delta-function in energy) cannot ignite. The behavior of the reacting system (quantities Q, I_{rad}, and P_n) is determined by the properties of the *secondary* migma, which has evolved, by virtue of a carefully designed injection process, into a bi-temperature migma. Such "plasma preparation" of 20–30 s is essential to facilitate ignition. (c) The system must be able to confine ions up to 10 MeV. (d) Diamagnetic well with $\beta \geq 0.9$ is essential. (e) Ignition is *not* possible in a *closed* system ($C = 0$). *Opening* of the loss cone ($C = 0.1$) *increases* the migma temperature owing to the escape of high-Z low-E_i ash, and makes the system ignite. (f) Migma never thermalizes if the tepid ion escape is balanced by the fuel and reaction product input.

6.2. Energetics, radioactivity, and neutronicism

(1) The d–^{3}He reaction. It undergoes steady state *self-ignition* with $Q \sim 10^5$; it is *nonradioactive*, with $R = (0.5 \pm 0.1)\%$, but *not quite aneutronic*, $N = (3.5 \pm 0.5)\%$. Polarized d's [29] would reduce N to $(1 \pm 1)\%$ (errors are systematic). Increasing the fuel injection ratio tends to decrease N to as low as $(3.5 \pm 3)\%$ with small reduction in reactor power output ("leaning-out effect", fig. 11).

(2) The ^{3}He–^{6}Li reaction. It evolves into the proton–^{3}He *chain* (1–2); and undergoes *driven ignition* with $Q \simeq 1.77$; it is *nonradioactive* with $R = (0.5 \pm 0.2)\%$ (all of it from tritium), and *nearly aneutronic*, with $N = (2 \pm 0.5)\%$ (fig. 12), but does not self-ignite, $Q < 2$.

We have not optimized this reaction, however, as we did d + ^{3}He; i.e., we did not study the leaning out effect.

The d + ^{3}He and ^{3}He + ^{3}He reactions contribute little to the Q values of the ^{3}He–^{6}Li chain because they are assumed to have flat cross sections up to 5 MeV.

(3) The ^{3}He + ^{3}He reaction. It is *absolutely nonradioactive*, $R = 0$; and *aneutronic*, $N = 0$, but undergoes *driven ignition* only, with $Q \simeq 1.6$.

6.3. Methods to improve simulation

(1) The Fokker–Planck transport code should be used instead of a code that computes the gross average at one point in space; (2) the "ersatz" computation of P_S should be replaced by an exact formula between P_S and local β; (3) knowledge of electron and ion motions due to the $\boldsymbol{E} \times \boldsymbol{B}$ effect is needed, which could lead to a magnetron effect and reduce all P_b and P_s; (4) transport processes should be included in the calculation of P_s; (5) more detailed model of the loss cone should be included.

6.4. Concluding remarks

The underlying assumption of this study is that a migma with $\beta \gtrsim 0.9$ is possible. In light of recent studies of high β migma equilibrium and stability [17–19], this assumption is deemed reasonable (table 1). We note that, while β for migma has the same dimensions as for plasma, it does not have the same physical meaning; migma β becomes greater than 0.9 at the ion densities already achieved in thermal plasmas ($n \sim 10^{14}$ cm^{-3}).

Acknowledgements

The authors are grateful to Stephen Tamor and Harold Furth for their important comments, and particularly to Joseph Norwood Jr., for his invaluable discussions, physics comments, and editorial aid.

References

[1] Cockroft and Walton, Proc. R. Soc. (London) A127 (1932) 229.
[2] J.D. Gordon et al., TRW Energy Div. Group TRW-FRE-006 and EPRI RP 1663-1 (1981) unpublished; S. Tamor, SAIC-85/3005/APPAT-63 (1986) unpublished.
[3] J.R. McNally Jr., Nucl. Fus. 11 (1971) 187; ibid, 18 (1978) 133.
[4] L. Ruby and T. Lung, Nucl. Sci. Eng. 69 (1979) 107.
[5] A. Harms and M. Heindler, Acta Phys. Austr. 52 (1980) 201.
[6] B. Maglich, Estimates of the proton and ^{3}He subsidy rates in the protonic chain fission of ^{6}Li, United Sci. report AEL-83-15 (January 1983).
[7] R. Macek and B. Maglich, Part. Accel. 1 (1970) 121.
[8] B. Maglich et al., Appl. Phys. Lett. 26 (1975) 609.
[9] B. Maglich, Migma Summer Study Group, MIG report (1973).
[10] J. Ferrer et al., Nucl. Instr. and Meth. 157 (1978) 269.
[11] D. Al Salameh et al., Phys. Rev. Lett. 54 (1985) 796.
[12] R.A. Miller, Nucl. Instr. and Meth. 119 (1975) 275.
[13] M. Emery, FEC reports 76-76 and 2-77 (1976, 1977).
[14] B. Maglich and R.A. Miller, Electron-Catalyzed Fast-Fusion Migmacell, Fusion Energy Summer Study Group, FESS-73-19 (Aug. 29, 1973); see eq. (10). See also: R.A. Miller, Extreme Diamagnetic Regime, FEC-13-74, and Diamagnetic Calculation, FEC-16-75 (1974, 1975).
[15] S. Channon et al., Phys. Rev. A17 (1978) 407.
[16] L. Lara and F. Gratton, Phys. Fluids 29 (1986) 2332.
[17] J. Norwood, Bull. Am. Phys. Soc. 31 (1986) 1557, United Sciences internal report AEL-87-10.
[18] J. Brandenburg, Bull. Am. Phys. Soc. 31 (1986) 1557.
[19] M. Blake, Bull. Am. Phys. Soc. 31 (1986) 1557.
[20] T. Simonen et al., Nucl. Fus. Suppl. 2 (1979) 389 (Proc. 7th Int. Conf. on Plasma Physics and Controlled Nuclear Fusion, Innsbruck (1978) (IAEA, Vienna, 1979) IAEA-CN-37/J-1).
[21] J.R. McNally, Nucl. Tech/Fus. 2 (1982) 9.

[22] J. Golden, Bull. Am. Phys. Soc. 31 (1986) 890 (United Sci. FEC 77-301).
[23] S. Tamor, Bull. Am. Phys. Soc., 31 (1986) 891; 31 (1986) 1557, Power Balance in Diamagnetic Migma, SAIC Report APPAT-85.
[24] H. Burkhardt, Nucl. Fus. 2 (1962) 1.
[25] D.L. Book, NRL Plasma Formulary 31-32 (1980).
[26] E.W. Rothe and J.R. McNally, FED, ORNL (April 17, 1980).
[27] S. Atzemi and B. Coppi, Comments Plasma Phys. 6 (1980) 77; B. Coppi, Phys. Scripta T2 (1982) 590.
[28] J. Santarius, Nucl. Fus. 27 (1987) 167.
[29] Shuy et al., Fus. Technol. 9 (1986) 459.
[30] D.L. Jessby and H.H. Towner, Proc. EPRI Review Meeting on Advanced Fuel Fusion, EPRI-ER-546-SR (1977) p. 275.
[31] J. Galambos et al., Nucl. Fus. 24 (1984) 739.
[32] C. Powell et al., 4th Review Meeting of Aneutronic Power Feasibility study group, paper no. 2 (1986).
[33] B. Maglich, ibid., paper no. 3.